ACS EARTH AND SPACE CHEMISTRY

Article

Cite This: ACS Earth Space Chem. 2019, 3, 2549−2558

http://pubs.acs.org/journal/aesccq

Compositional Evolution of Secondary Organic Aerosol as Temperature and Relative Humidity Cycle in Atmospherically Relevant Ranges

Zixu Zhao,[†] Chen Le,[‡,§] Qi Xu,[∥] Weihan Peng,[‡,§] Huanhuan Jiang,[⊥] Ying-Hsuan Lin,[∥,⊥] David R. Cocker, III,[‡,§] and Haofei Zhang*[,†,∥]

[†]Department of Chemistry, University of California, Riverside, California 92521, United States

[‡]Department of Chemical and Environmental Engineering, University of California, Riverside, California 92521, United States

[§]College of Engineering—Center for Environmental Research and Technology (CE-CERT), University of California, Riverside, California 92521, United States

[∥]Environmental Toxicology Graduate Program, University of California, Riverside, California 92521, United States

[⊥]Department of Environmental Sciences, University of California, Riverside, California 92521, United States

Supporting Information

ABSTRACT: Atmospheric secondary organic aerosols (SOA) play an important role in the global particulate matter budget, and their chemical compositions determine critical properties that impact radiative forcing and human health. During temporal and spatial transport, atmospheric particles undergo ambient temperature and relative humidity (RH) changes or cycles that may transform their chemical compositions. Here, we report compositional evolution of SOA from α-pinene ozonolysis in a smog chamber as the temperature and RH cycle within atmospherically relevant ranges (5−35 °C; 10−80% RH). The results suggest that the organic vapor condensation is limited during cooling, in contrast to volatility-based predictions, likely due to high viscosity of the α-pinene SOA particles and the potential enrichment of semivolatile products in the particle surface region. Combining a number of online and offline aerosol bulk and molecular-level measurements, we determine that particle-phase reactions occur reversibly and irreversibly throughout the temperature/RH cycles, substantially modifying concentrations of the SOA constituents and forming new products. Further, the presence of water is found to enhance the SOA O/C ratios prominently during cooling (high RH). These findings have important implications for understanding the chemical evolution of SOA in the atmosphere through their lifetime and long-range transport.

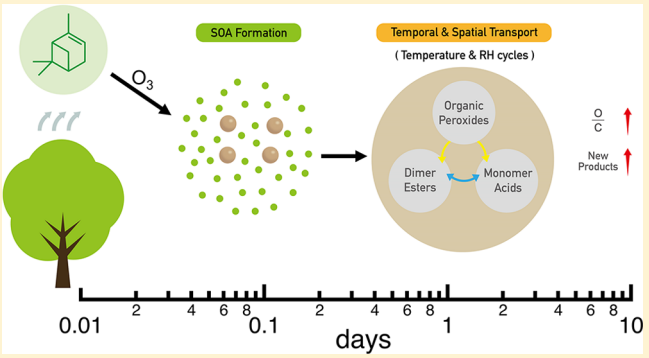

KEYWORDS: *α-pinene ozonolysis, gas-particle partitioning, aerosol viscosity, volatility, particle-phase reactions, liquid water content*

INTRODUCTION

Secondary organic aerosols (SOA) contribute to a significant fraction of atmospheric organic aerosols that impact the radiative forcing, air quality, and human health.[1−3] SOA are produced via the gas-phase oxidation of volatile organic compounds (VOC), resulting in a variety of low-volatility compounds that subsequently form new particles or condense onto existing particles.[4] During their lifetime of a few days to a week in the atmosphere,[5] SOA undergo daily cycles of diurnal temperature and relative humidity (RH) variations or long-range transport between the warmer planetary boundary layer and the cooler free troposphere.[6−8] The changing temperature and RH could effectively modify the volatilities of the SOA constituents and hence lead to active interactions with their gas-phase compartment (i.e., gas-particle partitioning).[9,10] Particle-phase chemistry may also be affected by the temperature and RH changes. Both processes could substantially evolve SOA compositions during their atmospheric lifetime and result in important climate, air quality, and health impacts.

Current air quality and climate models predict SOA mass and bulk compositions assuming that the gas-particle partitioning is under instantaneous thermodynamic equilibrium as temperature varies. Particle-phase reactions affected by the temperature and RH are usually not represented in the models. Environmental chambers are often used as a state-of-the-art tool for studying atmospheric SOA formation and evolution in laboratories,[11] but most existing chambers could

Received: August 26, 2019
Revised: October 9, 2019
Accepted: October 10, 2019
Published: October 10, 2019

DOI: 10.1021/acsearthspacechem.9b00232
ACS Earth Space Chem. 2019, 3, 2549−2558

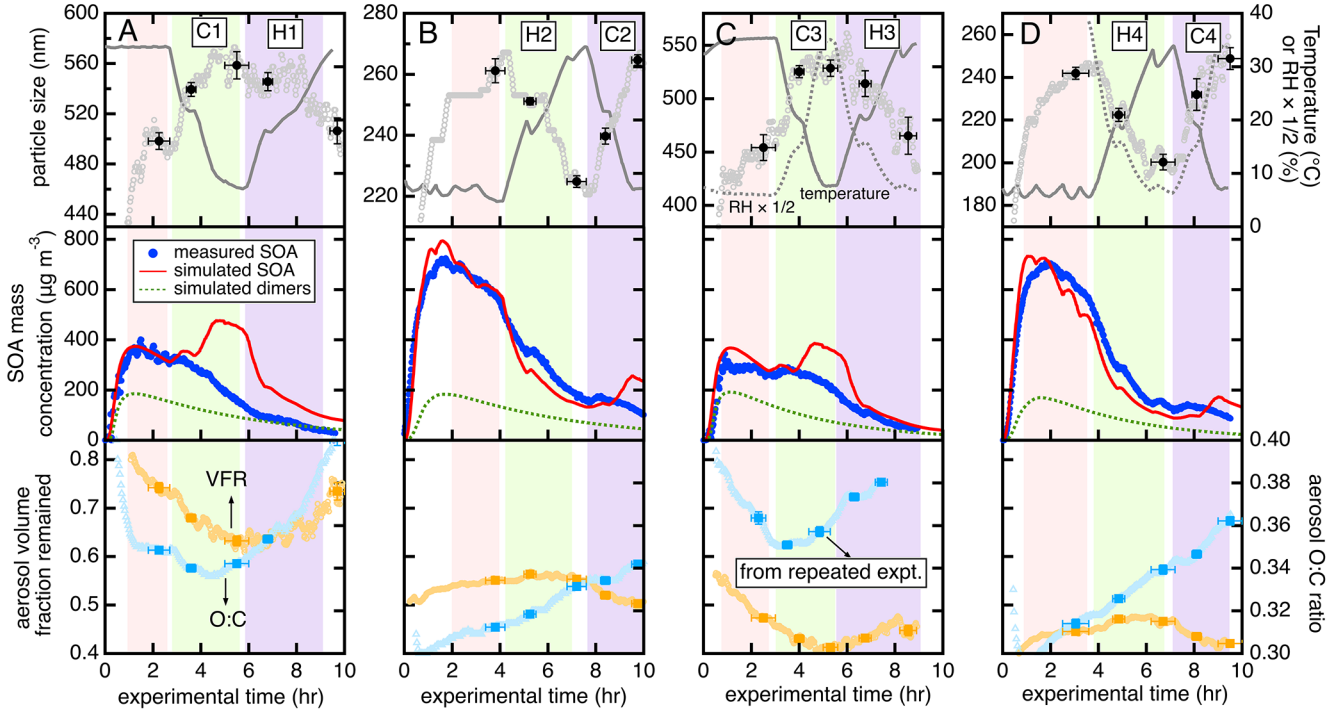

Figure 1. Time series of the temperature/RH cycling chamber experiments: (A) 35−5−35 °C (dry), (B) 5−35−5 °C (dry), (C) 35−5−35 °C (wet), and (D) 5−35−5 °C (wet). The top panels present the SOA size distribution modes (left axes, gray circles), temperature, and RH × 1/2 (right axes, gray solid and dashed curves, respectively). The middle panels show measured SOA mass concentration time series measured by the SMPS, with the volatility basis set (VBS)-simulated total SOA mass concentrations as well as the simulated dimers. The results shown here are wall-loss uncorrected. The bottom panels show measured particle volume fraction remained (VFR, left axes, orange symbols) and O/C ratios (right axes, blue symbols) of the SOA. The color-shaded regions represent the three aerosol sample collection time periods for each experiment. The O/C ratios shown in the (C) are from a different experiment than the other measurements, but with identical temperature and RH schemes. The symbols with error bars shown in all the plots are averaged values at stable temperatures. The four cooling and heating periods are termed "C1−C4" and "H1−H4", respectively.

not carry out experiments with temperature and RH cycles at long-enough time scales to approximate the atmospheric diurnal and spatial SOA evolution. Thus, how the physical properties and chemical compositions of SOA evolve during atmospheric temperature and RH cycles remains a critical yet unresolved question. One prior study has shown that as the temperature cycles between atmospherically relevant set points, the SOA mass could not be reproduced, suggesting insufficient condensation/evaporation, or irreversible particle-phase reactions, or both.[12] Growing evidence has demonstrated that atmospheric SOA could exist in distinct phase state and viscosity governed by RH,[13−17] and do not always reach equilibrium upon evaporation and condensation.[18−21] Further, common SOA constituents such as organic peroxides and some other types of oligomers were found to be labile and could decompose.[22−28] Some of the decomposition is induced by heat,[22,23,25,26] while some occurs at room temperature on the time scale of hours.[27,28] These evidence suggest that certain oligomers in SOA are thermally unstable and might decompose or react under atmospheric temperature ranges, provided sufficient time. Simultaneously, particle-phase accretion reactions also take place, in which RH may play crucial roles.[28−35] It is thus imperative to determine how SOA chemical compositions transform, as the bulk and on the molecular level, under temperature and RH changes representative of the real atmosphere.

In this work, we designed atmospherically relevant temperature/RH cycling (5−35 °C and 10−80% RH) experiments in an environmental chamber and studied the chemical transformation of α-pinene ozonolysis SOA. Coupling various online SOA bulk measurements and offline isomer-resolved comprehensive analyses, we report substantial SOA compositional evolution as a result of limited gas-particle partitioning and active particle-phase reactions during the temperature/RH cycles.

MATERIALS AND METHODS

Chamber Experiments. A series of temperature and RH cycled α-pinene ozonolysis experiments were performed in the UC Riverside/CE-CERT dual 90 m^3 Teflon environmental chambers. Details of the chambers have been described in previous work.[12,36] Briefly, the chambers are temperature and RH controlled with an operational time length of 12−16 h for each experiment. The chambers consist of a temperature-controlled enclosure that is continuously flushed with purified air. The experimental temperatures were determined by measurements at the centers of the chambers. Desired volumes of α-pinene (Sigma-Aldrich, ≥99%) were injected via a heated glass manifold flown by pure N_2. O_3 was generated from clean air by a Horiba OZG-UV-01 Ozone Generator Unit and injected into the chambers by a controlled flow rate for approximately 30 min. Carbon monoxide (CO) was injected directly from a CO cylinder (99.9% purity) to scavenge both the hydroxyl radicals (OH) and Criegee intermediates produced by the initial steps of α-pinene ozonolysis. Identical initial concentrations were used in all experiments with

DOI: 10.1021/acsearthspacechem.9b00232
ACS Earth Space Chem. 2019, 3, 2549−2558

approximately 250 ppb of α-pinene, 500 ppb of O_3, and 500 ppm of CO. The α-pinene and O_3 concentrations were set to be much higher than those in the real atmosphere, so that enough material could be collected (especially during the final stage of each experiment when most SOA particles had lost to the walls) for various and duplicated offline compositional analyses. In the experiments, initial α-pinene ozonolysis SOA were formed under a constant temperature of 35 or 5 °C; after most α-pinene was reacted (>95%, Figure S1) and SOA mass was stabilized, the temperature underwent a 35−5−35 °C cycle or a 5−35−5 °C cycle (Figure 1). RH remained <0.1% throughout the first two experiments (Figure 1A,B, hereafter referred to as "the dry experiments"); in the other two experiments with identical temperature cycles to the first two experiments, RH was also cycled between ∼10−80% with changing temperature by injecting water vapor before the experiments started (Figure 1C,D, hereafter referred to as "the wet experiments"). As temperature changed between 35 and 5 °C in each experiment, a ∼20 min pause was set at 20 °C. On average, the rates of temperature changes were ∼10 °C h^{-1} in all the experiments. For each experiment, three Teflon filter SOA samples were collected (Figure 1, color-shaded regions) at a constant flow rate (25 L min^{-1}): the first sample was collected during the initial constant temperature period after SOA mass was stable; the second sample during the first temperature change period between 35 and 5 °C; and the third sample during the temperature return period (see Figure 1 caption). Each of the filter samples was collected for 2−3 h and stored in the freezer at −20 °C right after collection.

Online Measurements. Concentrations of α-pinene and O_3 were measured by an Agilent 6890 GC-FID and a Dasibi O_3 analyzer, respectively. Particle size distribution and number concentrations were monitored by a custom built scanning mobility particle sizer (SMPS)[11] and a condensation particle counter (CPC, 3771, TSI Inc.). The SOA volatility was characterized by a house-built volatility tandem differential mobility analyzer (VT-DMA), which measures selected particle sizes before (D_{mi}) and after (D_{mf}) a Dekati thermodenuder at 100 °C for 17 s.[36] Volume fraction remained (VFR = D_{mf}^3/D_{mi}^3) represents the volatility of SOA. An Aerodyne high-resolution time-of-flight aerosol mass spectrometer (TOF-AMS)[37] was used to measure the bulk chemical compositions of SOA and determine the elemental ratios (i.e., O/C).[38]

SOA Compositions Measured by Offline Mass Spectrometry Techniques. Portions of the SOA filter samples were extracted for offline analyses by a gas chromatograph electron impact ionization mass spectrometer (GC−MS, Agilent Inc. 7890 GC and 5975 MSD)[35] and an electrospray ionization (ESI) ion mobility spectrometry time-of-flight mass spectrometer (IMS-TOF, Tofwerk Inc.)[39−41] to study the molecular compositions of the resultant SOA. The extraction procedures follow previous studies.[30,35,42] From the GC−MS measurements, four major α-pinene SOA tracers were detected and quantified, including pinonic acid ($C_{10}H_{16}O_3$), *cis*-pinic acid ($C_9H_{14}O_4$), 10-hydroxypinonic acid ($C_{10}H_{16}O_4$), and 3-hydroxyglutaric acid ($C_5H_8O_5$) (Figure S2).[43,44] From the detailed IMS-TOF measurements under both the positive and negative ion modes, we observed a number of polar oxygenated compounds with chemical formulas consistent with previously reported α-pinene SOA monomeric and dimeric products.[31,42,45−50] The ion mobility drift tube unit separates isomers in the SOA extracts and thus allow detections of individual species of interest.[39,40] The data from the IMS-TOF were analyzed using the Tofware v3.0.2 developed by Aerodyne Research, Inc. All the characterized α-pinene SOA products by the IMS-TOF are mapped in a drift-time (dt)−m/Q space shown in Figure S3, as well as mass defect plots shown in Figure S4. The variations of certain compounds (individual or grouped) during the temperature/RH cycles are discussed in the Results and Discussion section.

SOA Modeling. A thermodynamic model that assumes instantaneous gas-particle equilibrium was built using the VBS[10] to examine whether the behavior of α-pinene SOA produced in the chambers during the temperature/RH cycles is consistent with predictions based on the products' volatilities. The model used the Master Chemical Mechanism (MCM v3.2) to simulate the degradation of α-pinene.[51] The reacted α-pinene at each simulation time step is allocated to 9 volatility bins (the saturation concentration, C^* at 298 K ranging from 10^{-2} to 10^6 $\mu g\ m^{-3}$) with their empirical yields (Table S1). The C^* changing with temperature is represented by the Clausius−Clapeyron equation,[52] with the heat of vaporization (ΔH^{vap}) approximated by $\Delta H^{vap} = (-6 \log_{10}(C^*) + 100)$ kJ mol^{-1}. The VBS parametrization was from a prior study by Trump and Donahue,[52] which considered reversible oligomerization (monomer−oligomer equilibrium constant of 100 was used here). In addition, a model component representing vapor wall loss was implemented into the SOA model based on Zhang et al.[53] Note that the wall uptake rate constant of gaseous species is not volatility dependent, but the wall evaporation rate constant is. Hence, wall evaporation is enhanced at higher temperatures. Most of the vapor wall loss parameters are based on prior work except for the chamber specific ones. Sensitivity analyses suggested that different choices of the parameters (e.g., wall loss rate coefficient and the mass accommodation coefficient) within previously published ranges have little influence on simulation results. The key model parameters are presented in Table S1. The simulation results in comparison with measurements are presented in Figures 1 and S5.

RESULTS AND DISCUSSION

SOA Formation and Limited Vapor Condensation as Temperature and RH Cycle. Initial SOA formation from α-pinene ozonolysis exhibits clear temperature dependence (Figure 1; additional experiments starting at 20 °C are shown in Figure S5), consistent with prior work.[12,54,55] This trend is closely followed by the VBS simulations at all three temperatures, suggesting that the chosen VBS parameters are appropriate to model α-pinene ozonolysis SOA formation in these experiments, and the parametrized volatility distribution reasonably represents the formed products.[52] As the temperatures started to increase/decrease, the SOA size shrank/grew due to evaporation/condensation, as expected. During all the heating periods, SOA evaporation was reasonably captured by the model. However, it is surprising that during all the cooling periods, SOA mass growth was largely over predicted by the model, suggesting limited condensation of gaseous organic vapors onto the SOA particles under given experimental conditions. This effect is particularly substantial when the temperature drops below 20 °C (Figure 1A,C).

As we stated above, the VBS model reasonably simulates SOA at various initial temperatures, so it is unlikely that the condensation difference between the model and observations is caused by volatility distribution parametrization of the

DOI: 10.1021/acsearthspacechem.9b00232
ACS Earth Space Chem. 2019, 3, 2549−2558

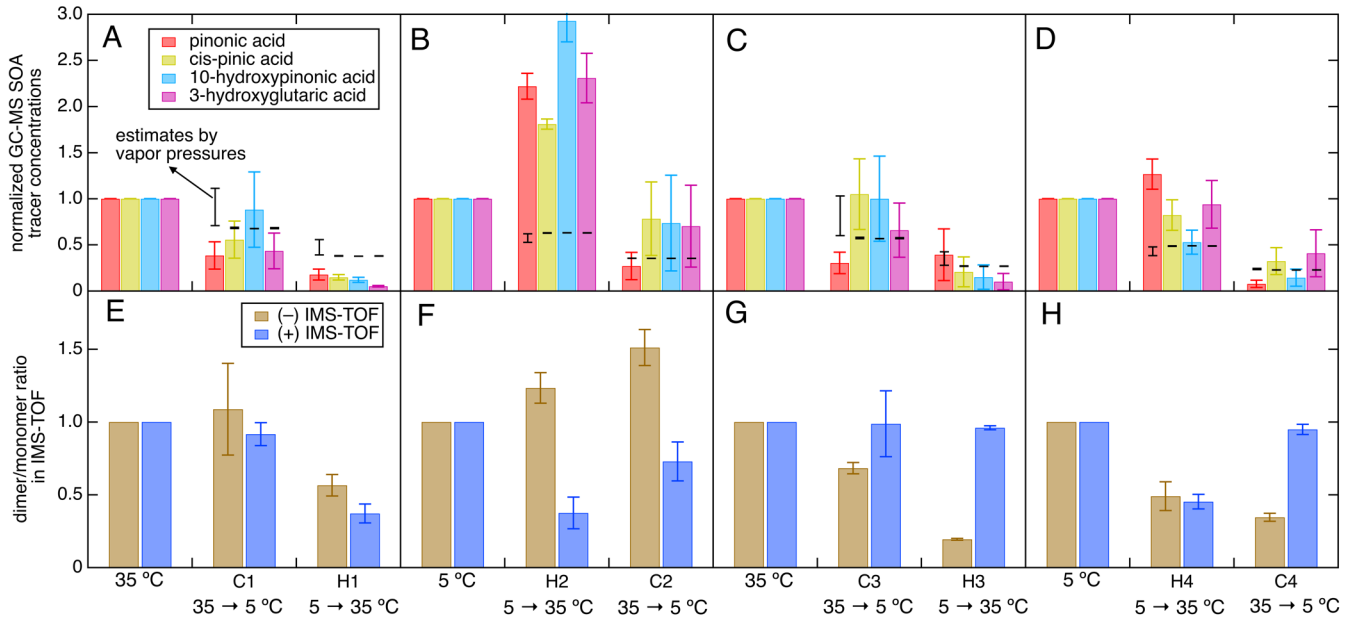

Figure 2. Chemical compositions of SOA from the same temperature/RH cycling experiments shown in Figure 1, measured by offline techniques. The top panels (A–D) present the mass concentrations of four typical α-pinene SOA tracers in the collected filter samples relative to the initial stable temperature periods measured by the GC–MS. The black error bars shown with the measurements are simulated relative abundance of these SOA tracers due only to gas-particle partitioning and wall losses (assuming that they are not involved in any particle-phase reactions). The bottom panels (E–H) are relative ratios of representative dimers to monomers (Figure S3) measured by the IMS-TOF in both the negative and positive ion modes.

products. Vapor wall loss is also unlikely to explain the gaps since we have incorporated this process explicitly in the model, and vapor wall loss is usually considered to have less influence on α-pinene SOA systems due to the fast oxidation and high SOA yields.[53,56] A higher likelihood is that the SOA particles were highly viscous, especially in the dry experiments,[14] and under the studied high mass loading, significant fractions of semivolatile organic compounds (SVOC) might have partitioned to the particle phase. However, their partitioning was likely later than the lower volatility species (LVOC), which should have condensed earlier when the SOA mass was lower. This is evidenced by the O/C ratios shown in Figure 1: at the beginning of all the experiments, the SOA O/C ratios started high (comprised mostly of more oxidized LVOC) and followed a substantial decrease (partitioning of less oxidized SVOC). The later-partitioned SVOCs are likely confined at near particle surface region (except for the experiment starting at 5 °C and 80% RH), impeding further partitioning of the gas-phase SVOC.[14] Thus, a condensation limitation is expected. This effect might also explain the rapid evaporation during heating: the evaporation of SVOC from the particle surface was likely not limited by the less volatile and more viscous materials that were in the particle bulk. At higher RH (i.e., C3 in Figure 1), SOA particles could be less viscous, and thus the better mixing of partitioned SVOC allowed gas-phase SVOC condensation to occur more readily. Further, the relatively smaller measurement-model difference at higher RH might be partially owing to the uptake of water-soluble oxidized VOCs from the gas phase. The overall higher O/C ratios and volatilities of SOA in the two wet experiments compared to the dry experiments support that sizable oxidized VOCs were present in the SOA under high RH.

Although the observed condensation limitation appears in contradiction to previously reported evaporation limitation of α-pinene SOA,[18,20] we note that their observed early evaporation (likely SVOC) was rather rapid and that the limitation was mostly for the lower volatility compounds. In that regard, the results are in fact consistent. Nevertheless, it is unclear whether the condensation limitation observed here is also applicable when SOA mass loadings are lower and the partitioning behavior of SVOC is different. Future studies using lower concentrations are warranted to examine the role of SOA mass loading on organic vapor condensation.

Change of SOA Bulk Compositions and Volatilities as Temperature and RH Cycle. Despite the limited condensation of gaseous organic vapors during cooling in the temperature/RH cycles, if most of the physical (gas-particle partitioning) and chemical (particle-phase reactions) processes were reversible, the SOA bulk compositions should have exhibited time series toward reversible trajectories to certain degree as the temperature/RH cycles completed. However, the SOA O/C ratio shown in Figures 1 and S5 (bottom panels) indicates otherwise. After SOA mass stabilized and the temperature/RH cycles started, the O/C ratio increased during all the heating periods, consistent with that more volatile and less oxidized products evaporated. In contrast, increased O/C was also observed during all cooling periods, after an initial drop or flat (indicative of condensation of less oxidized species). This suggests that particle-phase reactions lead to more oxidized products (discussed later in the text) since there was no OH to heterogeneously oxidize the SOA in the chamber. In addition, the VFR data show somewhat different extents of reversibility of the SOA volatility. The VFR in both the "35–5–35 °C" experiments approximately returned to the original levels, while that in the experiments started at 5 °C (Figure 1) or 20 °C (Figure S5) ended with higher volatility (lower VFR). The volatility enhancements in the "5–35–5 °C" experiments are resulted by that volatility

DOI: 10.1021/acsearthspacechem.9b00232
ACS Earth Space Chem. 2019, 3, 2549–2558

increased during cooling as it should, but did not decrease during heating (when the particles were expected to be less volatile after evaporating more volatile compounds). These results suggest that during heating to 35 °C, irreversible particle-phase reactions such as oligomer decomposition into monomers might have occurred that eventually lead to more volatile SOA.[22,23] This process offsets the effect of evaporation-induced volatility decrease. For the experiments starting at 35 °C (Figures 1A,C), however, such effect was not as apparent, likely because the oligomers that are prone to decomposition during heating were already decomposed before the cooling started. Therefore, the SOA volatility changed more expectedly during the later heating periods (H1 and H3). These hypotheses are supported by molecular-level compositional analyses discussed in the later section. Thus, far, the bulk measurements of SOA using the TOF-AMS and VT-DMA have shown evidence of particle-phase reactions in all the temperature/RH cycling experiments. Further, the SOA became more oxidized through the temperature/RH cycles regardless of the temperature/RH schemes, in the absence of gas-phase OH.

SOA Molecular Compositions Indicate Particle-Phase Reactions. To further examine the detailed SOA molecular compositions and hence the particle-phase reactions during the temperature/RH cycling experiments, we used the GC-MS and IMS-TOF to study the variation of individual and grouped α-pinene SOA species. The top panels in Figure 2 show the relative mass concentrations (to the initial stable temperature periods) of the four major α-pinene SOA tracers measured by the GC−MS. Also shown in Figure 2 with the GC−MS measurements are the predicted relative abundances of the same SOA tracers based only on gas-particle partitioning and wall losses (black uncertainty bars in the Figure 2 top panels). The gas-particle partitioning coefficients of the four compounds were estimated using calculated vapor pressures from several group contribution methods and measurements (Table S2).[57−61] Although different methods result in very distinct vapor pressure estimates, the high particle mass loadings used in this study lead to very little variation in partitioning behavior between different vapor pressures. Only for the more volatile pinonic acid, there is a noticeable range of uncertainty. The small uncertainties increase our confidence that there must have been particle-phase reactions involving these well-known α-pinene SOA tracers during the temperature/RH cycles. Particularly, during the H2 heating period, these tracers are substantially larger than predicted (as high as 3 times more than the original stable temperature periods), suggesting their formation from particle-phase reactions, likely dimer decomposition. The enhancement during H4 is not as substantial as H2 (only for pinonic acid, *cis*-pinic acid, and 3-hydroxyglutaric acid, to a lesser degree) because the existence of water likely has already limited/decomposed dimer production in the initial SOA formation step, consistent with the VFR results that the dry experiments produced less-volatile SOA than the wet under the same initial temperatures. The absolute mass concentrations of the GC−MS results shown in Table S3 support these interpretations that the major SOA monomers are 2−7 times more abundant in the wet experiment during the stable temperature periods. The strong dimer decomposition was not observed in the other two heating periods either (H1 and H3), which followed initial high temperature (35 °C) and subsequent cooling. Consistent with the volatility results discussed above, the dimer decomposition may have already occurred during the initial SOA formation periods (under 35 °C) in these two experiments. During the other periods, some of these major α-pinene SOA tracers also deviated from predictions, to a lesser degree. This implies that these compounds, as well as most other species in the SOA, are constantly involved in particle-phase reactions (formation and consumption). The changing temperatures have likely affected the kinetics of these processes, eventually leading to different SOA compositions through a temperature/RH cycle.

To determine whether particle-phase reactions occur to the majority of the SOA species, we studied the dominant product ions observed in the IMS-TOF (see Figure S3) that have been reported as major α-pinene SOA constituents in previous work, including both monomers and dimers.[31,42,45,46,48,50,62−65] In the negative ion mode, the major products are monomeric carboxylic acids and dimeric esters. In the positive ion mode, since existing work has been scarce,[42,65] we focused on dominant ions with chemical formula of $C_{8-10}H_{12-18}O_{3-10}$ (monomers) and $C_{16-20}H_{26-32}O_{4-13}$ (dimers), as plausible products of α-pinene SOA. It has been suggested that in the (+) ESI, the ions detected as sodiated adducts $[M + Na]^+$ are likely multifunctional species containing (hydro)peroxides and esters.[42] We summed the intensities of dimers and monomers in both ion modes, respectively, and compared the dimer-to-monomer ratios of the SOA collected on filter samples during the temperature/RH cycling experiments (Figure 2, bottom panels). Overall, very distinct trends were observed between different experiments and different temperature/RH schemes. Below are a few important observations to note. First, in the 5−35−5 °C experiments (Figure 2F,H), the dimer-to-monomer ratio in the positive ion mode largely decreased during heating (H2 and H4), but almost came back during cooling (C2 and C4), indicating a reversible process. Accompanied by this in the dry experiment, an enhancement of dimer-to-monomer ratio in the negative ion mode was observed during both H2 and C2. Coupling these observations to the enhanced monomers during H2 in the GC−MS results indicates that the SOA formed at 5 °C (dry) contained substantial organic peroxides, which were largely decomposed at 35 °C into both monomers (such as the tracers measured in GC−MS) and dimer esters. This mechanism is likely an irreversible process. A similar mechanism has been proposed by Zhang et al. in a previous study.[50] In both the wet experiments in the chamber, the dimer-to-monomer ratios consistently decreased in the negative ion mode throughout the experiments regardless of the temperature scheme (Figure 2G,H), suggesting the dominance of ester hydrolysis when the particles contained liquid water.[30] More accurate and quantitative interpretation was not possible using the current techniques, but the combination of all the above measurements together has clearly demonstrated that active and complex particle-phase reactions (reversible and irreversible) occurred during the studied temperature/RH cycling experiments. Further, although our measurements of dimers are not quantitative, previous work[66] and the simulations shown in Figure 1 are consistent that dimers could contribute significantly to α-pinene SOA. Thus, we suggest that the reactions proposed here involving dimers could largely impact the SOA compositions during the temperature/RH cycles.

Formation of New Products through Particle-Phase Reactions during the Temperature/RH Cycles. The particle-phase reactions demonstrated here have largely transformed the SOA molecular compositions during the

DOI: 10.1021/acsearthspacechem.9b00232
ACS Earth Space Chem. 2019, 3, 2549−2558

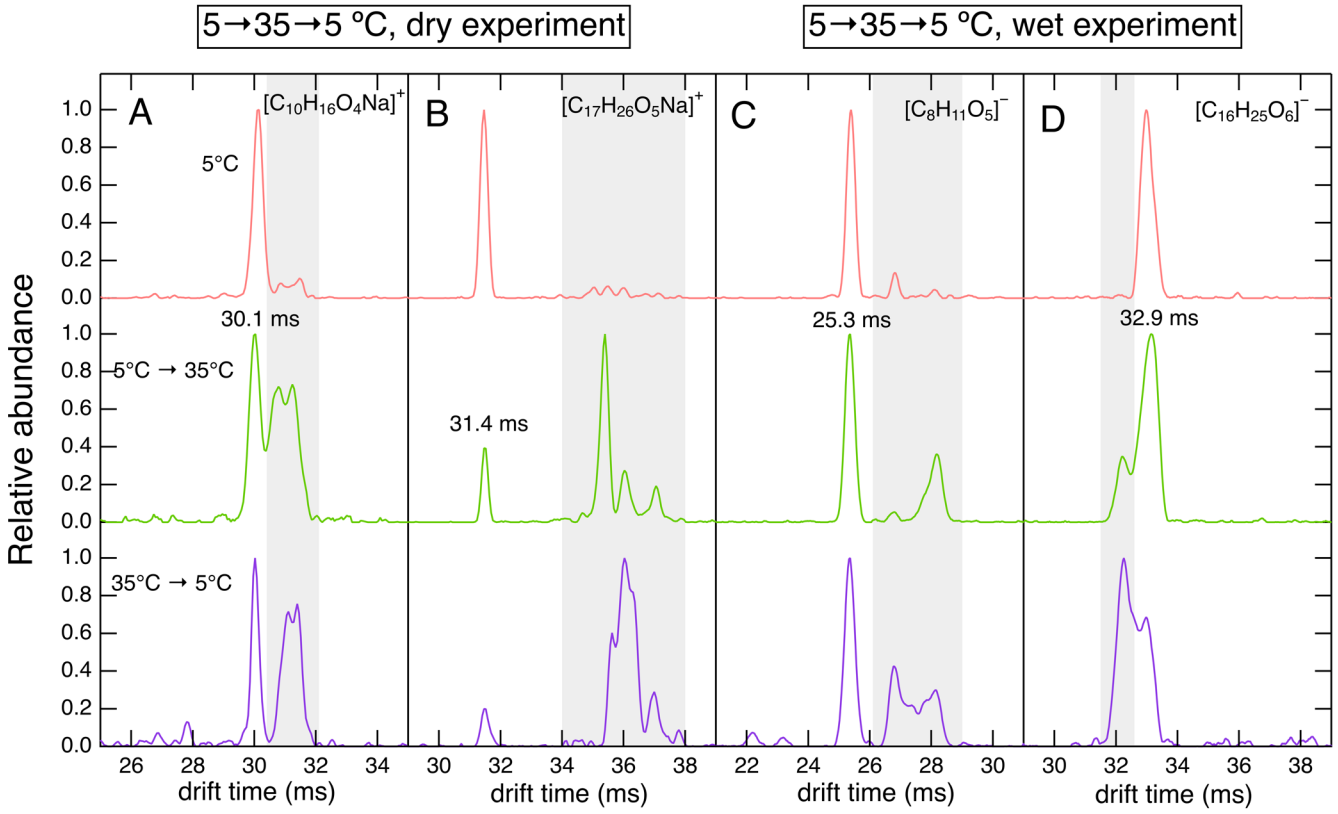

Figure 3. Ion mobility spectra ("driftgrams") of four representative molecular ions: (A) $[C_{10}H_{16}O_4Na]^+$, (B) $[C_{17}H_{26}O_5Na]^+$, (C) $[C_8H_{11}O_5]^-$, and (D) $[C_{16}H_{25}O_6]^-$. (A,B) "5−35−5 °C" dry experiment; (C,D) "5−35−5 °C" wet experiment. Drift times of the peaks originally present in the first samples (top panel) are labeled. Newly formed peaks during temperature cycles (two bottom panels) rise in the gray-shaded regions.

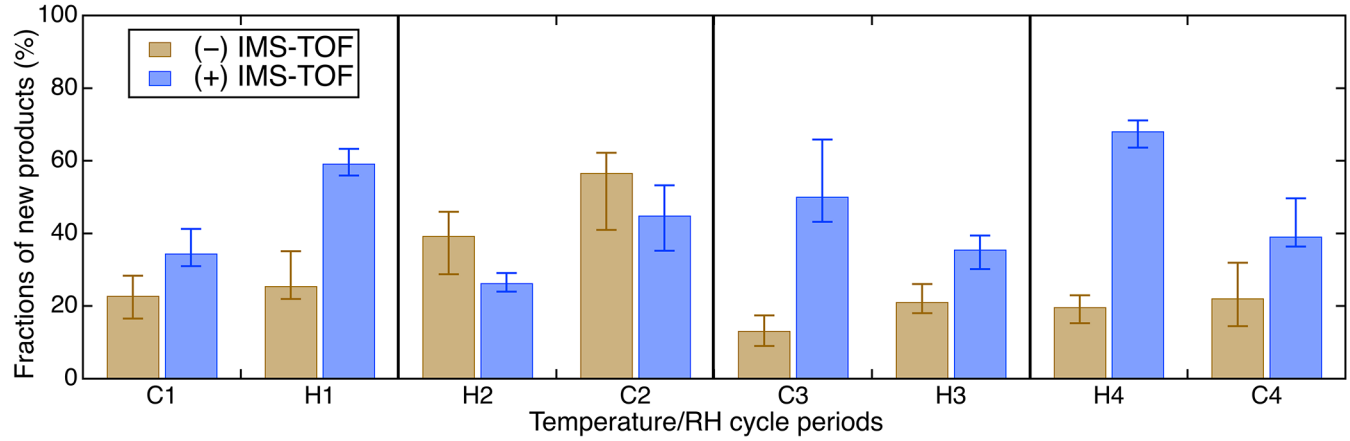

Figure 4. Fractions of new isomeric products (intensities in the IMS-TOF) during each temperature change period in comparison to the initial SOA. The error bars represent uncertainties using different allowances of ion mobility drift time shift.

temperature/RH cycling experiments. This includes changes in abundance of initial SOA constituents (discussed above), as well as formation of new species that further enhance the complexity of SOA. Typical ESI-MS measurements of SOA compositions cannot unambiguously determine new products due to the complexity in SOA and uncertain matrix effect, but with the isomers separated by the IMS at each individual m/Q, whether new products are formed can be clearly pictured. Figure 3 illustrates several examples of new isomeric product formation during the temperature/RH cycles based on the isomer-resolved capability of the IMS-TOF. The molecular ions shown in the driftgrams have been previously reported as major constituents of α-pinene ozonolysis SOA.[42,50,64] Before the temperature/RH cycles started (Figure 3, top panel), only one major peak was present at each of these chemical formulas. The smaller peaks are all below the estimated confidence levels. As heating started, high abundances of new peaks rise in the dirftgrams, suggesting substantial formation of new isomers at these molecular masses via particle-phase reactions during the temperature/RH cycles. For all the 380 molecular ions (Figure S3) analyzed by the IMS-TOF, the summed intensities of new products during temperature/RH cycles were

DOI: 10.1021/acsearthspacechem.9b00232
ACS Earth Space Chem. 2019, 3, 2549−2558

compared with those of all products (Figure 4). We determine that on the order of 20−60% of the major ion intensities were formed during the temperature/RH cycles, varied largely by different temperature/RH schemes and whether water vapor was present. Although ESI-based techniques are considered less quantitative due to matrix effects, relative intensities of ions at the same m/Q are likely proportional to their concentrations. Thus, with new products observed at many of the major molecular ions, the ratios we reported here can approximate the actual mass fractions in the SOA. Note that in most cases (except for the (+) IMS-TOF results for the wet experiments), the new products are more abundant during the temperature return periods, indicating irreversible processes leading to the new products. Although detailed particle-phase reaction mechanisms accounting for the observations warrant further studies, these findings already provide important evidence that the SOA compositions may become more complicated than its initial form at the molecular level after undergoing particle-phase reactions led by temperature and RH changes and cycles. However, the quantitative fractions of new products need to be interpreted with caution because part of them could be simply due to time (some particle-phase reactions are slow), rather than temperature and RH. Future work is warranted to perform control experiments under constant temperatures/RH and hence differentiate the roles of time vs cycling temperatures and RH in the observed substantial compositional variation.

After discussing the various possible particle-phase reactions, it is probably worthwhile to integrate the results and rethink the observed SOA bulk composition evolution. Through the temperature/RH cycles, we have provided evidence suggesting reversible and irreversible dimer decomposition, more prominently during the heating periods. Ester hydrolysis was also apparent when water was present. In the literature, these decomposition processes were considered only when particles are heated at above 100 °C and higher[67] or in the presence of strong acidity.[68] Here we show that these reactions could occur at much lower temperature and without acidity for SOA-relevant compounds, if sufficient time is provided (on the order of hours). From these processes, the monomer products may evaporate to the gas phase, especially with decreasing particle mass loading and/or increasing temperatures. The evaporation might also play a role, driving the dimer decomposition kinetics. As a result of the evaporation, the SOA bulk O/C ratios increased, as observed from the experiments. However, these processes described above are unlikely reconciled with the increased O/C ratios observed during the cooling periods. As we discussed earlier, the SVOC condensation, despite being limited by the high SOA viscosity, should have lowered the overall SOA O/C ratios during cooling, which has barely occurred. We note that the O/C ratio enhancement rate during cooling was faster when water was present (10.3×10^{-3} h^{-1}) than in the dry experiments (5.8×10^{-3} h^{-1}). The difference is likely attributed to water-involved reactions. For example, the above-mentioned ester hydrolysis and other aqueous-phase reactions[69] could convert the oxygen from the water molecules into organic moieties and hence increase the SOA O/C ratios. This water-induced difference, by ∼0.01 over 2 h, is approximately equivalent to that 10% of all monomers (assuming all are C_{10}) and 20% of all dimers (assuming all are C_{20}) add an oxygen per molecule. This is a significant change overall, suggesting the important role of water in particle-phase chemistry. However, it is still unclear what caused the O/C ratio increase during cooling in the dry experiments. A likely explanation is that there was still substantial evaporation of SVOC during cooling due to the decreasing SOA mass. Other possibilities cannot be ruled out, but would involve adding oxygen from O_2 or O_3, which require particle-phase radical reactions or heterogeneous ozonolysis of C═C formed in the SOA.

Atmospheric Implications. Accurately predicting SOA mass concentrations is a critical task in atmospheric models that require appropriate representations of both SOA formation and their evolution through temporal and spatial transport. The evolution usually involves a combined result of three recognized processes: (1) heterogeneous oxidative aging, (2) gas-particle partitioning, and (3) particle-phase reactions. Heterogeneous oxidative aging depends mainly on gas-phase oxidant concentrations and has been extensively examined in laboratory studies to provide parametrized results for model implementation.[70−72] The two latter processes are determined, in part, by ambient temperature and RH that could change dramatically during the SOA lifetime. How these changes affect the SOA evolution and how models represent this evolution, however, have not been studied. Although the initial high SOA mass loading (∼300−700 μg m^{-3}) and rapid temperature/RH cycling rates (∼10 °C/23% per hour) used in this work are unrealistic for the real atmosphere, as the first study of its kind to our best knowledge, this work presents important evidence and highlights the necessity to study SOA compositional evolution caused by temperature and RH cycles under more relevant conditions in future studies.

We first reported the limited condensation of organic vapors during cooling compared to volatility-based predictions. This observation implicates that, for the real atmosphere, as ambient temperature decreases during nighttime or aerosols are transported to cold environment, the limited condensation of SVOC and more volatile species could result in faster oxidation in the gas phase and forming more oxidized products more efficiently. In the free troposphere where temperatures are even lower, organics more volatile than SVOC stay in the gas phase longer than expected and thus more readily form low-volatile compounds. Further, we determined that during the temperature and RH cycles particle-phase reactions substantially occur, reversibly and irreversibly, modifying the concentrations of the SOA constituents and producing new products to a great degree (20−60% new products through one temperature cycle, Figure 4). The presence of water during cooling (high RH) was also suggested to substantially participate in particle-phase chemistry. Atmospheric SOA usually experience multiple of these cycles during their lifetime, and hence, the chemical compositions of aged SOA could be even more distinct from the freshly formed SOA than presented here. Therefore, the various particle-phase reactions and the temperature/RH influences demonstrated in the present study should be implemented in current models to better represent the evolution of atmospheric SOA through their temporal and spatial transport.

■ ASSOCIATED CONTENT

Supporting Information

The Supporting Information is available free of charge on the ACS Publications website at DOI: 10.1021/acsearthspacechem.9b00232.

DOI: 10.1021/acsearthspacechem.9b00232
ACS Earth Space Chem. 2019, 3, 2549−2558

VOC degradation data (Figure S1), GC−MS chromatogram (Figure S2), IMS−TOF diagrams (Figure S3), mass defect plots (Figure S4), additional chamber experiment results (Figure S5), detailed parameters for the simulations and vapor pressure estimates (Tables S1 and S2), mass concentrations of GC−MS results (Table S3) (PDF)

AUTHOR INFORMATION

Corresponding Author

*E-mail: haofei.zhang@ucr.edu.

ORCID

Huanhuan Jiang: 0000-0002-5581-375X

Ying-Hsuan Lin: 0000-0001-8904-1287

Haofei Zhang: 0000-0002-7936-4493

Notes

The authors declare no competing financial interest.

REFERENCES

(1) Pope, C. A.; Dockery, D. W. Health Effects of Fine Particulate Air Pollution: Lines That Connect. *J. Air Waste Manage. Assoc.* **2006**, *56* (6), 709−742.

(2) Hallquist, M.; Wenger, J. C.; Baltensperger, U.; Rudich, Y.; Simpson, D.; Claeys, M.; Dommen, J.; Donahue, N. M.; George, C.; Goldstein, A. H.; Hamilton, J. F.; Herrmann, H.; Hoffmann, T.; Iinuma, Y.; Jang, M.; Jenkin, M. E.; Jimenez, J. L.; Kiendler-Scharr, A.; Maenhaut, W.; McFiggans, G.; Mentel, T. F.; Monod, A.; Prévôt, A. S. H.; Seinfeld, J. H.; Surratt, J. D.; Szmigielski, R.; Wildt, J. The Formation, Properties and Impact of Secondary Organic Aerosol: Current and Emerging Issues. *Atmos. Chem. Phys.* **2009**, *9* (14), 5155−5236.

(3) IPCC. *Fifth Assessment Report, Climate Change*; Intergovernmental Panel on Climate Change. 2013.

(4) Kroll, J. H.; Seinfeld, J. H. Chemistry of Secondary Organic Aerosol: Formation and Evolution of Low-Volatility Organics in the Atmosphere. *Atmos. Environ.* **2008**, *42* (16), 3593−3624.

(5) Hodzic, A.; Kasibhatla, P. S.; Jo, D. S.; Cappa, C. D.; Jimenez, J. L.; Madronich, S.; Park, R. J. Rethinking the Global Secondary Organic Aerosol (SOA) Budget: Stronger Production, Faster Removal, Shorter Lifetime. *Atmos. Chem. Phys.* **2016**, *16* (12), 7917−7941.

(6) Fast, J. D.; Allan, J.; Bahreini, R.; Craven, J.; Emmons, L.; Ferrare, R.; Hayes, P. L.; Hodzic, A.; Holloway, J.; Hostetler, C.; Jimenez, J. L.; Jonsson, H.; Liu, S.; Liu, Y.; Metcalf, A.; Middlebrook, A.; Nowak, J.; Pekour, M.; Perring, A.; Russell, L.; Sedlacek, A.; Seinfeld, J.; Setyan, A.; Shilling, J.; Shrivastava, M.; Springston, S.; Song, C.; Subramanian, R.; Taylor, J. W.; Vinoj, V.; Yang, Q.; Zaveri, R. A.; Zhang, Q. Modeling Regional Aerosol and Aerosol Precursor Variability over California and Its Sensitivity to Emissions and Long-Range Transport During the 2010 CalNex and CARES Campaigns. *Atmos. Chem. Phys.* **2014**, *14* (18), 10013−10060.

(7) Rinaldi, M.; Gilardoni, S.; Paglione, M.; Sandrini, S.; Fuzzi, S.; Massoli, P.; Bonasoni, P.; Cristofanelli, P.; Marinoni, A.; Poluzzi, V.; Decesari, S. Organic Aerosol Evolution and Transport Observed at Mt. Cimone (2165 M A.S.L.), Italy, During the PEGASOS Campaign. *Atmos. Chem. Phys.* **2015**, *15* (19), 11327−11340.

(8) Zhou, S.; Collier, S.; Jaffe, D. A.; Zhang, Q. Free Tropospheric Aerosols at the Mt. bachelor Observatory: More Oxidized and Higher Sulfate Content Compared to Boundary Layer Aerosols. *Atmos. Chem. Phys.* **2019**, *19* (3), 1571−1585.

(9) Pankow, J. F. An Absorption Model of the Gas/Aerosol Partitioning Involved in the Formation of Secondary Organic Aerosol. *Atmos. Environ.* **1994**, *28* (2), 189−193.

(10) Donahue, N. M.; Robinson, A. L.; Stanier, C. O.; Pandis, S. N. Coupled Partitioning, Dilution, and Chemical Aging of Semivolatile Organics. *Environ. Sci. Technol.* **2006**, *40* (8), 2635−2643.

(11) Cocker, D. R.; Flagan, R. C.; Seinfeld, J. H. State-of-the-Art Chamber Facility for Studying Atmospheric Aerosol Chemistry. *Environ. Sci. Technol.* **2001**, *35* (12), 2594−2601.

(12) Warren, B.; Austin, R. L.; Cocker, D. R. Temperature Dependence of Secondary Organic Aerosol. *Atmos. Environ.* **2009**, *43* (22), 3548−3555.

(13) Virtanen, A.; Joutsensaari, J.; Koop, T.; Kannosto, J.; Yli-Pirilä, P.; Leskinen, J.; Mäkelä, J. M.; Holopainen, J. K.; Pöschl, U.; Kulmala, M.; Worsnop, D. R.; Laaksonen, A. An Amorphous Solid State of Biogenic Secondary Organic Aerosol Particles. *Nature* **2010**, *467*, 824.

(14) Renbaum-Wolff, L.; Grayson, J. W.; Bateman, A. P.; Kuwata, M.; Sellier, M.; Murray, B. J.; Shilling, J. E.; Martin, S. T.; Bertram, A. K. Viscosity of α-Pinene Secondary Organic Material and Implications for Particle Growth and Reactivity. *Proc. Natl. Acad. Sci. U. S. A.* **2013**, *110* (20), 8014.

(15) Abramson, E.; Imre, D.; Beránek, J.; Wilson, J.; Zelenyuk, A. Experimental Determination of Chemical Diffusion within Secondary Organic Aerosol Particles. *Phys. Chem. Chem. Phys.* **2013**, *15* (8), 2983−2991.

(16) Järvinen, E.; Ignatius, K.; Nichman, L.; Kristensen, T. B.; Fuchs, C.; Hoyle, C. R.; Höppel, N.; Corbin, J. C.; Craven, J.; Duplissy, J.; Ehrhart, S.; El Haddad, I.; Frege, C.; Gordon, H.; Jokinen, T.; Kallinger, P.; Kirkby, J.; Kiselev, A.; Naumann, K. H.; Petäjä, T.; Pinterich, T.; Prevot, A. S. H.; Saathoff, H.; Schiebel, T.; Sengupta, K.; Simon, M.; Slowik, J. G.; Tröstl, J.; Virtanen, A.; Vochezer, P.; Vogt, S.; Wagner, A. C.; Wagner, R.; Williamson, C.; Winkler, P. M.; Yan, C.; Baltensperger, U.; Donahue, N. M.; Flagan, R. C.; Gallagher, M.; Hansel, A.; Kulmala, M.; Stratmann, F.; Worsnop, D. R.; Möhler, O.; Leisner, T.; Schnaiter, M. Observation of Viscosity Transition in α-Pinene Secondary Organic Aerosol. *Atmos. Chem. Phys.* **2016**, *16* (7), 4423−4438.

(17) King, M. D.; Rennie, A. R.; Thompson, K. C.; Fisher, F. N.; Dong, C. C.; Thomas, R. K.; Pfrang, C.; Hughes, A. V. Oxidation of Oleic Acid at the Air−Water Interface and Its Potential Effects on Cloud Critical Supersaturations. *Phys. Chem. Chem. Phys.* **2009**, *11* (35), 7699−7707.

(18) Vaden, T. D.; Imre, D.; Beránek, J.; Shrivastava, M.; Zelenyuk, A. Evaporation Kinetics and Phase of Laboratory and Ambient Secondary Organic Aerosol. *Proc. Natl. Acad. Sci. U. S. A.* **2011**, *108* (6), 2190−2195.

(19) Cappa, C. D.; Wilson, K. R. Evolution of Organic Aerosol Mass Spectra upon Heating: Implications for Oa Phase and Partitioning Behavior. *Atmos. Chem. Phys.* **2011**, *11* (5), 1895−1911.

(20) Wilson, J.; Imre, D.; Beránek, J.; Shrivastava, M.; Zelenyuk, A. Evaporation Kinetics of Laboratory-Generated Secondary Organic Aerosols at Elevated Relative Humidity. *Environ. Sci. Technol.* **2015**, *49* (1), 243−249.

(21) Perraud, V.; Bruns, E. A.; Ezell, M. J.; Johnson, S. N.; Yu, Y.; Alexander, M. L.; Zelenyuk, A.; Imre, D.; Chang, W. L.; Dabdub, D.; Pankow, J. F.; Finlayson-Pitts, B. J. Nonequilibrium Atmospheric Secondary Organic Aerosol Formation and Growth. *Proc. Natl. Acad. Sci. U. S. A.* **2012**, *109* (8), 2836.

(22) Hall, W. A.; Johnston, M. V. The Thermal-Stability of Oligomers in Alpha-Pinene Secondary Organic Aerosol. *Aerosol Sci. Technol.* **2012**, *46* (9), 983−989.

(23) D'Ambro, E. L.; Schobesberger, S.; Zaveri, R. A.; Shilling, J. E.; Lee, B. H.; Lopez-Hilfiker, F. D.; Mohr, C.; Thornton, J. A. Isothermal Evaporation of α-Pinene Ozonolysis SOA: Volatility, Phase State, and Oligomeric Composition. *ACS Earth Space Chem.* **2018**, *2* (10), 1058−1067.

(24) Stark, H.; Yatavelli, R. L. N.; Thompson, S. L.; Kang, H.; Krechmer, J. E.; Kimmel, J. R.; Palm, B. B.; Hu, W.; Hayes, P. L.; Day, D. A.; Campuzano-Jost, P.; Canagaratna, M. R.; Jayne, J. T.; Worsnop, D. R.; Jimenez, J. L. Impact of Thermal Decomposition on Thermal Desorption Instruments: Advantage of Thermogram Analysis for Quantifying Volatility Distributions of Organic Species. *Environ. Sci. Technol.* **2017**, *51* (15), 8491−8500.

DOI: 10.1021/acsearthspacechem.9b00232
ACS Earth Space Chem. 2019, 3, 2549−2558

(25) Claflin, M. S.; Ziemann, P. J. Thermal Desorption Behavior of Hemiacetal, Acetal, Ether, and Ester Oligomers. *Aerosol Sci. Technol.* **2019**, *53* (4), 473−484.
(26) Lopez-Hilfiker, F. D.; Mohr, C.; Ehn, M.; Rubach, F.; Kleist, E.; Wildt, J.; Mentel, T. F.; Carrasquillo, A. J.; Daumit, K. E.; Hunter, J. F.; Kroll, J. H.; Worsnop, D. R.; Thornton, J. A. Phase Partitioning and Volatility of Secondary Organic Aerosol Components Formed from α-Pinene Ozonolysis and OH Oxidation: The Importance of Accretion Products and Other Low Volatility Compounds. *Atmos. Chem. Phys.* **2015**, *15* (14), 7765−7776.
(27) Krapf, M.; El Haddad, I.; Bruns, E. A.; Molteni, U.; Daellenbach, K. R.; Prevot, A. S.H.; Baltensperger, U.; Dommen, J. Labile Peroxides in Secondary Organic Aerosol. *Chem.* **2016**, *1* (4), 603−616.
(28) Pagonis, D.; Ziemann, P. J. Chemistry of Hydroperoxycarbonyls in Secondary Organic Aerosol. *Aerosol Sci. Technol.* **2018**, *52* (10), 1178−1193.
(29) Barsanti, K. C.; Pankow, J. F. Thermodynamics of the Formation of Atmospheric Organic Particulate Matter by Accretion Reactions—Part 3: Carboxylic and Dicarboxylic Acids. *Atmos. Environ.* **2006**, *40* (34), 6676−6686.
(30) Zhang, H.; Surratt, J. D.; Lin, Y. H.; Bapat, J.; Kamens, R. M. Effect of Relative Humidity on SOA Formation from Isoprene/NO Photooxidation: Enhancement of 2-Methylglyceric Acid and Its Corresponding Oligoesters under Dry Conditions. *Atmos. Chem. Phys.* **2011**, *11* (13), 6411−6424.
(31) Kristensen, K.; Enggrob, K. L.; King, S. M.; Worton, D. R.; Platt, S. M.; Mortensen, R.; Rosenoern, T.; Surratt, J. D.; Bilde, M.; Goldstein, A. H.; Glasius, M. Formation and Occurrence of Dimer Esters of Pinene Oxidation Products in Atmospheric Aerosols. *Atmos. Chem. Phys.* **2013**, *13* (7), 3763−3776.
(32) Jang, M.; Czoschke, N. M.; Lee, S.; Kamens, R. M. Heterogeneous Atmospheric Aerosol Production by Acid-Catalyzed Particle-Phase Reactions. *Science* **2002**, *298* (5594), 814.
(33) Hall, W. A.; Johnston, M. V. Oligomer Formation Pathways in Secondary Organic Aerosol from MS and MS/MS Measurements with High Mass Accuracy and Resolving Power. *J. Am. Soc. Mass Spectrom.* **2012**, *23* (6), 1097−1108.
(34) Yasmeen, F.; Sauret, N.; Gal, J. F.; Maria, P. C.; Massi, L.; Maenhaut, W.; Claeys, M. Characterization of Oligomers from Methylglyoxal under Dark Conditions: A Pathway to Produce Secondary Organic Aerosol through Cloud Processing During Nighttime. *Atmos. Chem. Phys.* **2010**, *10* (8), 3803−3812.
(35) Zhao, Z.; Xu, Q.; Yang, X.; Zhang, H. Heterogeneous Ozonolysis of Endocyclic Unsaturated Organic Aerosol Proxies: Implications for Criegee Intermediate Dynamics and Later-Generation Reactions. *ACS Earth Space Chem.* **2019**, *3* (3), 344−356.
(36) Clark, C. H.; Kacarab, M.; Nakao, S.; Asa-Awuku, A.; Sato, K.; Cocker, D. R. Temperature Effects on Secondary Organic Aerosol (SOA) from the Dark Ozonolysis and Photo-Oxidation of Isoprene. *Environ. Sci. Technol.* **2016**, *50* (11), 5564−5571.
(37) DeCarlo, P. F.; Dunlea, E. J.; Kimmel, J. R.; Aiken, A. C.; Sueper, D.; Crounse, J.; Wennberg, P. O.; Emmons, L.; Shinozuka, Y.; Clarke, A.; Zhou, J.; Tomlinson, J.; Collins, D. R.; Knapp, D.; Weinheimer, A. J.; Montzka, D. D.; Campos, T.; Jimenez, J. L. Fast Airborne Aerosol Size and Chemistry Measurements above Mexico City and Central Mexico During the MILAGRO Campaign. *Atmos. Chem. Phys.* **2008**, *8* (14), 4027−4048.
(38) Canagaratna, M. R.; Jimenez, J. L.; Kroll, J. H.; Chen, Q.; Kessler, S. H.; Massoli, P.; Hildebrandt Ruiz, L.; Fortner, E.; Williams, L. R.; Wilson, K. R.; Surratt, J. D.; Donahue, N. M.; Jayne, J. T.; Worsnop, D. R. Elemental Ratio Measurements of Organic Compounds Using Aerosol Mass Spectrometry: Characterization, Improved Calibration, and Implications. *Atmos. Chem. Phys.* **2015**, *15* (1), 253−272.
(39) Krechmer, J. E.; Groessl, M.; Zhang, X.; Junninen, H.; Massoli, P.; Lambe, A. T.; Kimmel, J. R.; Cubison, M. J.; Graf, S.; Lin, Y. H.; Budisulistiorini, S. H.; Zhang, H.; Surratt, J. D.; Knochenmuss, R.; Jayne, J. T.; Worsnop, D. R.; Jimenez, J. L.; Canagaratna, M. R. Ion Mobility Spectrometry−Mass Spectrometry (IMS−MS) for on- and Offline Analysis of Atmospheric Gas and Aerosol Species. *Atmos. Meas. Tech.* **2016**, *9* (7), 3245−3262.
(40) Zhang, X.; Krechmer, J. E.; Groessl, M.; Xu, W.; Graf, S.; Cubison, M.; Jayne, J. T.; Jimenez, J. L.; Worsnop, D. R.; Canagaratna, M. R. A Novel Framework for Molecular Characterization of Atmospherically Relevant Organic Compounds Based on Collision Cross Section and Mass-to-Charge Ratio. *Atmos. Chem. Phys.* **2016**, *16* (20), 12945−12959.
(41) Zhang, X.; Zhang, H.; Xu, W.; Tyndall, G. S.; Orlando, J. J.; Jayne, J. T.; Worsnop, D. R.; Canagaratna, M. R. Molecular Characterization of Alkyl Nitrates in Atmospheric Aerosols by Ion Mobility Mass Spectrometry. *Atmos. Meas. Technol. Discuss.* **2019**, *2019*, 1−21.
(42) Zhang, X.; Lambe, A. T.; Upshur, M. A.; Brooks, W. A.; Gray Bé, A.; Thomson, R. J.; Geiger, F. M.; Surratt, J. D.; Zhang, Z.; Gold, A.; Graf, S.; Cubison, M. J.; Groessl, M.; Jayne, J. T.; Worsnop, D. R.; Canagaratna, M. R. Highly Oxygenated Multifunctional Compounds in α-Pinene Secondary Organic Aerosol. *Environ. Sci. Technol.* **2017**, *51* (11), 5932−5940.
(43) Zhang, H.; Yee, L. D.; Lee, B. H.; Curtis, M. P.; Worton, D. R.; Isaacman-VanWertz, G.; Offenberg, J. H.; Lewandowski, M.; Kleindienst, T. E.; Beaver, M. R.; Holder, A. L.; Lonneman, W. A.; Docherty, K. S.; Jaoui, M.; Pye, H. O. T.; Hu, W.; Day, D. A.; Campuzano-Jost, P.; Jimenez, J. L.; Guo, H.; Weber, R. J.; de Gouw, J.; Koss, A. R.; Edgerton, E. S.; Brune, W.; Mohr, C.; Lopez-Hilfiker, F. D.; Lutz, A.; Kreisberg, N. M.; Spielman, S. R.; Hering, S. V.; Wilson, K. R.; Thornton, J. A.; Goldstein, A. H. Monoterpenes Are the Largest Source of Summertime Organic Aerosol in the Southeastern United States. *Proc. Natl. Acad. Sci. U. S. A.* **2018**, *115* (9), 2038.
(44) Yu, J.; Flagan, R. C.; Seinfeld, J. H. Identification of Products Containing -COOH, -OH, and -CO in Atmospheric Oxidation of Hydrocarbons. *Environ. Sci. Technol.* **1998**, *32* (16), 2357−2370.
(45) Claeys, M.; Szmigielski, R.; Vermeylen, R.; Wang, W.; Shalamzari, M. S.; Maenhaut, W. In *Tracers for Biogenic Secondary Organic Aerosol from α-Pinene and Related Monoterpenes: An Overview*; Rudziński, I. B. a. K. J., Ed. NATO Science for Peace and Security Series C-Environmental Security: Dordrecht, Netherlands, 2013; pp 227−238.
(46) Claeys, M.; Iinuma, Y.; Szmigielski, R.; Surratt, J. D.; Blockhuys, F.; Van Alsenoy, C.; Böge, O.; Sierau, B.; Gómez-González, Y.; Vermeylen, R.; Van der Veken, P.; Shahgholi, M.; Chan, A. W. H.; Herrmann, H.; Seinfeld, J. H.; Maenhaut, W. Terpenylic Acid and Related Compounds from the Oxidation of α-Pinene: Implications for New Particle Formation and Growth above Forests. *Environ. Sci. Technol.* **2009**, *43* (18), 6976−6982.
(47) Claeys, M.; Szmigielski, R.; Kourtchev, I.; Van der Veken, P.; Vermeylen, R.; Maenhaut, W.; Jaoui, M.; Kleindienst, T. E.; Lewandowski, M.; Offenberg, J. H.; Edney, E. O. Hydroxydicarboxylic Acids: Markers for Secondary Organic Aerosol from the Photooxidation of α-Pinene. *Environ. Sci. Technol.* **2007**, *41* (5), 1628−1634.
(48) Yasmeen, F.; Szmigielski, R.; Vermeylen, R.; Gómez-González, Y.; Surratt, J. D.; Chan, A. W. H.; Seinfeld, J. H.; Maenhaut, W.; Claeys, M. Mass Spectrometric Characterization of Isomeric Terpenoic Acids from the Oxidation of α-Pinene, β-Pinene, d-Limonene, and Δ3-Carene in Fine Forest Aerosol. *J. Mass Spectrom.* **2011**, *46* (4), 425−442.
(49) Kristensen, K.; Cui, T.; Zhang, H.; Gold, A.; Glasius, M.; Surratt, J. D. Dimers in α-Pinene Secondary Organic Aerosol: Effect of Hydroxyl Radical, Ozone, Relative Humidity and Aerosol Acidity. *Atmos. Chem. Phys.* **2014**, *14* (8), 4201−4218.
(50) Zhang, X.; McVay, R. C.; Huang, D. D.; Dalleska, N. F.; Aumont, B.; Flagan, R. C.; Seinfeld, J. H. Formation and Evolution of Molecular Products in α-Pinene Secondary Organic Aerosol. *Proc. Natl. Acad. Sci. U. S. A.* **2015**, *112* (46), 14168−14173.
(51) Saunders, S. M.; Jenkin, M. E.; Derwent, R. G.; Pilling, M. J. Protocol for the Development of the Master Chemical Mechanism,

DOI: 10.1021/acsearthspacechem.9b00232
ACS Earth Space Chem. 2019, 3, 2549−2558

MCM v3 (Part A): Tropospheric Degradation of Non-Aromatic Volatile Organic Compounds. *Atmos. Chem. Phys.* **2003**, *3* (1), 161−180.
(52) Trump, E. R.; Donahue, N. M. Oligomer Formation within Secondary Organic Aerosols: Equilibrium and Dynamic Considerations. *Atmos. Chem. Phys.* **2014**, *14* (7), 3691−3701.
(53) Zhang, X.; Cappa, C. D.; Jathar, S. H.; McVay, R. C.; Ensberg, J. J.; Kleeman, M. J.; Seinfeld, J. H. Influence of Vapor Wall Loss in Laboratory Chambers on Yields of Secondary Organic Aerosol. *Proc. Natl. Acad. Sci. U. S. A.* **2014**, *111* (16), 5802.
(54) Stanier, C. O.; Pathak, R. K.; Pandis, S. N. Measurements of the Volatility of Aerosols from α-Pinene Ozonolysis. *Environ. Sci. Technol.* **2007**, *41* (8), 2756−2763.
(55) Pathak, R. K.; Stanier, C. O.; Donahue, N. M.; Pandis, S. N. Ozonolysis of α-Pinene at Atmospherically Relevant Concentrations: Temperature Dependence of Aerosol Mass Fractions (Yields). *J. Geophys. Res.* **2007**, *112* (D3), 007436.
(56) Nah, T.; McVay, R. C.; Zhang, X.; Boyd, C. M.; Seinfeld, J. H.; Ng, N. L. Influence of Seed Aerosol Surface Area and Oxidation Rate on Vapor Wall Deposition and SOA Mass Yields: A Case Study with α-Pinene Ozonolysis. *Atmos. Chem. Phys.* **2016**, *16* (14), 9361−9379.
(57) Bilde, M.; Pandis, S. N. Evaporation Rates and Vapor Pressures of Individual Aerosol Species Formed in the Atmospheric Oxidation of α- and β-Pinene. *Environ. Sci. Technol.* **2001**, *35* (16), 3344−3349.
(58) Pankow, J. F.; Asher, W. E. Simpol.1: A Simple Group Contribution Method for Predicting Vapor Pressures and Enthalpies of Vaporization of Multifunctional Organic Compounds. *Atmos. Chem. Phys.* **2008**, *8* (10), 2773−2796.
(59) Nannoolal, Y.; Rarey, J.; Ramjugernath, D.; Cordes, W. Estimation of Pure Component Properties: Part 1. Estimation of the Normal Boiling Point of Non-Electrolyte Organic Compounds via Group Contributions and Group Interactions. *Fluid Phase Equilib.* **2004**, *226*, 45−63.
(60) Nannoolal, Y.; Rarey, J.; Ramjugernath, D. Estimation of Pure Component Properties: Part 3. Estimation of the Vapor Pressure of Non-Electrolyte Organic Compounds via Group Contributions and Group Interactions. *Fluid Phase Equilib.* **2008**, *269* (1), 117−133.
(61) Moller, B.; Rarey, J.; Ramjugernath, D. Estimation of the Vapour Pressure of Non-Electrolyte Organic Compounds via Group Contributions and Group Interactions. *J. Mol. Liq.* **2008**, *143* (1), 52−63.
(62) Yasmeen, F.; Vermeylen, R.; Maurin, N.; Perraudin, E.; Doussin, J.-F.; Claeys, M. Characterisation of Tracers for Aging of α-Pinene Secondary Organic Aerosol Using Liquid Chromatography/Negative Ion Electrospray Ionisation Mass Spectrometry. *Environ. Chem.* **2012**, *9* (3), 236−246.
(63) Yasmeen, F.; Vermeylen, R.; Szmigielski, R.; Iinuma, Y.; Böge, O.; Herrmann, H.; Maenhaut, W.; Claeys, M. Terpenylic Acid and Related Compounds: Precursors for Dimers in Secondary Organic Aerosol from the Ozonolysis of α- and β-Pinene. *Atmos. Chem. Phys.* **2010**, *10* (19), 9383−9392.
(64) Kourtchev, I.; Doussin, J. F.; Giorio, C.; Mahon, B.; Wilson, E. M.; Maurin, N.; Pangui, E.; Venables, D. S.; Wenger, J. C.; Kalberer, M. Molecular Composition of Fresh and Aged Secondary Organic Aerosol from a Mixture of Biogenic Volatile Compounds: A High-Resolution Mass Spectrometry Study. *Atmos. Chem. Phys.* **2015**, *15* (10), 5683−5695.
(65) Camredon, M.; Hamilton, J. F.; Alam, M. S.; Wyche, K. P.; Carr, T.; White, I. R.; Monks, P. S.; Rickard, A. R.; Bloss, W. J. Distribution of Gaseous and Particulate Organic Composition During Dark α-Pinene Ozonolysis. *Atmos. Chem. Phys.* **2010**, *10* (6), 2893−2917.
(66) Hall, W. A.; Johnston, M. V. Oligomer Content of α-Pinene Secondary Organic Aerosol. *Aerosol Sci. Technol.* **2011**, *45* (1), 37−45.
(67) Cappa, C. D.; Jimenez, J. L. Quantitative Estimates of the Volatility of Ambient Organic Aerosol. *Atmos. Chem. Phys.* **2010**, *10* (12), 5409−5424.
(68) Mabey, W.; Mill, T. Critical Review of Hydrolysis of Organic Compounds in Water under Environmental Conditions. *J. Phys. Chem. Ref. Data* **1978**, *7* (2), 383−415.
(69) Herrmann, H.; Schaefer, T.; Tilgner, A.; Styler, S. A.; Weller, C.; Teich, M.; Otto, T. Tropospheric Aqueous-Phase Chemistry: Kinetics, Mechanisms, and Its Coupling to a Changing Gas Phase. *Chem. Rev.* **2015**, *115* (10), 4259−4334.
(70) Rudich, Y.; Donahue, N. M.; Mentel, T. F. Aging of Organic Aerosol: Bridging the Gap between Laboratory and Field Studies. *Annu. Rev. Phys. Chem.* **2007**, *58* (1), 321−352.
(71) George, I. J.; Slowik, J.; Abbatt, J. P. D. Chemical Aging of Ambient Organic Aerosol from Heterogeneous Reaction with Hydroxyl Radicals. *Geophys. Res. Lett.* **2008**, *35* (13), 033884.
(72) Donahue, N. M.; Henry, K. M.; Mentel, T. F.; Kiendler-Scharr, A.; Spindler, C.; Bohn, B.; Brauers, T.; Dorn, H. P.; Fuchs, H.; Tillmann, R.; Wahner, A.; Saathoff, H.; Naumann, K.-H.; Möhler, O.; Leisner, T.; Müller, L.; Reinnig, M.-C.; Hoffmann, T.; Salo, K.; Hallquist, M.; Frosch, M.; Bilde, M.; Tritscher, T.; Barmet, P.; Praplan, A. P.; DeCarlo, P. F.; Dommen, J.; Prévôt, A. S. H.; Baltensperger, U. Aging of Biogenic Secondary Organic Aerosol via Gas-Phase OH Radical Reactions. *Proc. Natl. Acad. Sci. U. S. A.* **2012**, *109* (34), 13503−13508.

DOI: 10.1021/acsearthspacechem.9b00232
ACS Earth Space Chem. 2019, 3, 2549−2558